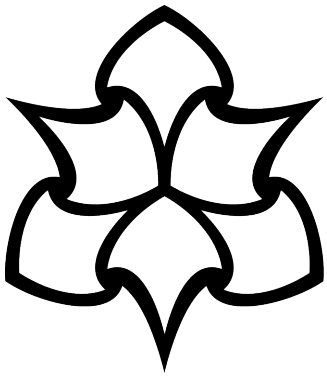

Manchester Metropolitan University

Sarkar, Subhasish, Baranwal, Rishav Kumar, Mukherjee, Arghya, Koley, Ishita, Biswas, Chanchal, Haider, Julfikar ORCID logoORCID: https://orcid.org/0000-0001-7010-8285 and Majumdar, Gautam (2020) Optimisation & minimisation of corrosion rate of electroless Ni-Co-P coating. Advances in Materials and Processing Technologies, 6 (3). pp. 487-508. ISSN 2374-068X

Downloaded from: https://e-space.mmu.ac.uk/624864/

Version: Accepted Version

Publisher: Informa UK Limited

DOI: https://doi.org/10.1080/2374068x.2019.1709326

Please cite the published version

https://e-space.mmu.ac.uk

Optimization and Minimization of Corrosion Rate of Electroless Ni-Co-P Coating

[1]Subhasish Sarkar, [1*]Rishav Kumar Baranwal, [1]Arghya Mukherjee, [2]Ishita Koley, [3]Chanchal Biswas, [4]Julfikar Haider, [1]Gautam Majumdar

[1]Department of Mechanical Engineering, Jadavpur University, Kolkata-700032, India

[2]Department of Metallurgical and Materials Engineering, IIEST, Shibpur-711101, India

[3]Department of Metallurgical and Materials Engineering, Jadavpur University, Kolkata-700032, India

[4]Department of Engineering and Advanced Materials and Surface Engineering Research Centre, Manchester Metropolitan University, Manchester, United Kingdom

*Corresponding Author's Email Id: rishavbaranwal22@gmail.com

Abstract
Electroless Ni-Co–P alloy coatings were deposited to decrease the corrosion rate of the copper substrate. Central Composite Design (CCD) was employed through Design Expert Software to establish optimized deposition parameters, which produces a coating having high corrosion resistance. CCD has also been employed to determine the effect of various process parameters namely concentration of cobalt sulfate ($CoSO_4.7H_2O$) solution (10-20 gm/cc), concentration of sodium hypophosphite ($NaH_2PO_2.H_2O$) solution (20-30 gm/cc) and bath temperature (80-90°C). The corrosion rate was determined by the Potential Dynamic test in 3.5% NaCl solution and the Tafel plot was used to determine the corrosion current density for each coated substrate. On the corrosion response of the coatings, the most significant interactions and important factors were identified using ANOVA analysis. The regression analysis showed a good fit of the experimental data through the second-order polynomial model with a coefficient of determination (R^2) value of 0.9531 and a model F-value of 22.57. 15 g/L of Cobalt Sulphate, 30 g/L of Sodium Hypophosphite and 80ºC of bath temperature were found out to be the optimum conditions of bath deposition to obtain a corrosion rate of 0.535 µm/Y.

Keywords
Electroless Ni-Co–P coating, Corrosion, SEM, XRD, Central Composite Design (CCD)

1. INTRODUCTION

Electroless coatings, since its discovery some 60 years ago by Brenner and Riddell, have found extensive use in industrial applications. Electroless coating deposition is an autocatalytic technique that has the ability to deposit coating uniformly on complex geometries and can be easily customized to fulfill the requirements for a particular application. The most significant function of autocatalytically deposited coatings is to provide protection against corrosion and wear [1]. The growth of industry demands enhanced performance of the parts against corrosion and wear which is a universal challenge. Electroless nickel is an engineered coating that is normally used because of its excellent corrosion and wear resistance as well as other functional properties like lubrication based on the hydrophobic/hydrophilic nature of the coating, electromagnetic shielding by using Cobalt, highly improved hardness by using chromates, etc. Hence, it is widely used in different industrial fields such as chemical industries, automobiles, electronics, aerospace, etc. [2,3]

Corrosion has proved to be hazardous for all the existing materials on the earth's surface. Corrosion occurs due to the development of a potential difference between the surface of the material and the surrounding atmosphere. Corrosion affects the performance of critical parts and products such as biomedical devices [4,5] and specially manufactured precision parts like mechanical and electronic instruments [6–8]. Corrosion has been proved to be fatal and costly for the industries and end users as they have to set a plan for regular preventative maintenance and replacement of the corroded parts. More recently, NACE International14 has released a global impact study, which states that the estimated global cost of corrosion is USD $2.5 trillion, which is equivalent to roughly 3.4 percent of the global Gross Domestic Product (GDP). In India alone, the direct cost of corrosion was estimated as USD 26.1 billion or 2.4 percent of India's GDP. The study also estimated that global savings between 15-35 percent of the cost of damage, or between USD 375-875 billion could be possible by implementing best corrosion prevention practices and measures. Therefore, it is necessary to prevent corrosion of metals in order to reduce global economic loss. Copper has proved to be a material of high importance due to its daily use along with its applications and superior qualities. However, the surface of copper gets corroded with time which reduces its operational life and performance [9]. Hence different ways have been developed to improve the corrosion resistance or protect the surface from being corroded [10,11]. One of the popular ways to improve corrosion resistance is the application of functional coating [12,13].

The electroless coating is classified as pure nickel, Electroless Nickel (EN) alloy coating, EN composite coating, and EN nano-coating. The present work concentrates on EN alloy coating which can be further classified into binary, ternary and quaternary alloy coatings [14]. Ternary coatings can provide solutions for improving the properties of the binary coatings [15] by incorporating an additional alloying element. Surface Properties of the EN coatings can also be modified with the help of annealing [16,17]. However, with the application of heat treatment, the amorphous state of the as-deposited binary coated material changes into the crystalline state [4,18] which decreases the corrosion resistance offered by the coating. Thus, in order to improve the corrosion resistance of the binary coatings, one of the

ways suggested in the literature which proved to be effective, is to introduce a third element in the coating forming a ternary alloy [19]. Development of electroless nickel poly-alloy deposits is considered to be the most effective method in order to improve the properties of electroless Ni-P deposits by adding cobalt, copper or tungsten. Cobalt is generally used as it possesses high-temperature wear and corrosion resistance [20,21]. By controlling the Ni/Co ratio of deposits, the corrosion resistance of Ni-Co-P deposits could be best coordinated. Deposits with P content over 8 wt% has an amorphous structure and deposit with P content less than 4 wt% has a crystal structure. Cobalt addition to the Ni-P deposit of amorphous structure can improve the corrosion resistance. It is realized that Co can increase the plating rate in amorphous deposits but decrease the plating rate in mix-crystalline deposits [18].

The objective of this study is to improve the corrosion resistance of electroless Ni-P coating as a sacrificial and protective layer on the copper substrate by the incorporation of cobalt ions. This sacrificial layer is prepared in an electroless bath by controlling different deposition parameters such as the concentration of bath solutions and bath temperature. However, these parameters need to be optimized as only a particular combination of the input parameters results in the best corrosion resistance. The optimization techniques employed are based on different mathematical modeling [22–24]. During the time of synthesis, pre-treatment was done followed by cleaning and activation of the sample and then the sample was placed in the bath solution for 1 hr to obtain the sample coated with a thin bright layer of Ni-Co-P alloy coating. The improved hardness of the Ni-Co-P coating has been optimized using a different optimization technique by Sarkar *et al.* [25]. However, no study exists in the literature on the optimization of the corrosion rate of Ni-Co-P coating. This study presents corrosion test results and discusses the mechanism behind lower corrosion rates in Ni-Co-P coating. In this work, the concentration of Cobalt Sulphate, Sodium Hypophosphite, and bath temperature have been considered as the three parameters which have been optimized using Central Composite Design (CCD) of experiment. Now, in order to determine the significant parameters in this process, Analysis of Variance (ANOVA), a powerful mathematical tool has been used to analyze the residuals and outliers, and also to examine the competency of the developed model. Further the Ni-Co-P coated substrates, deposited in the optimized condition have been characterized using Optical microscope, Scanning Electron Microscope (SEM) and Energy Dispersive X-ray (EDX) analysis in order to analyze the surface morphology and the elemental composition of the as-deposited coated substrates.

2. EXPERIMENTAL DETAILS

2.1. Substrate preparation

In the present work, rectangular copper foils were used as a substrate for coating them with electroless Ni-Co-P. Rolled copper foil of 0.1 mm thickness was purchased from LobaChemie with 99% purity and cut into standard rectangular samples with a dimension of 15 mm×15 mm. Firstly, the substrates were cleaned using distilled water. Subsequently, acid pickling was performed on the substrate to remove any oxide layer, carbonized hydrocarbon and different impurities that might be present on the surface of the substrate. For acid pickling, standard samples were dipped into 25% Hydrochloric acid (HCl) for 10 minutes at room temperature. After that, substrates were dipped again in distilled water to remove the acid layer on them and then the substrates were dipped into the Palladium Chloride ($PdCl_2$) solution which was pre-heated to 55 °C for activation. Finally, the samples were taken out and once again cleaned in distilled water for 1 min before transferring them to the electroless bath.

2.2. Preparation of coating

Nickel sulfate ($NiSO_4.6H_2O$), cobalt sulfate ($CoSO_4.7H_2O$), sodium hypophosphite ($NaH_2PO_2.H_2O$), tri-sodium citrate dihydrate ($Na_3C_6H_5O_7.2H_2O$) and ammonium sulfate ($(NH_4)_2SO_4$) were used for the preparation of the bath. Along with the appropriate bath temperature, the pH level was kept constant throughout the coating process so that the deposition develops significantly. The bath temperature of the solution was continuously monitored with the help of a thermometer which was placed in the plating bath. The compositions of the bath and process parameters are tabulated in Table 1.

Table 1: Chemical composition and process parameter of electroless bath for Ni-Co-P coating deposition

Factors	Value
Nickel sulfate hexahydrate	25 (gm lit^{-1})
Cobalt sulfate heptahydrate	6.56 - 23.44(gm lit^{-1})
Sodium Hypophosphite	23.44 - 33.33 (gm lit^{-1})
Trisodium citrate dihydrate	15 (gm lit^{-1})
Ammonium sulfate	10 (gm lit^{-1})
Bath temperature	76.44 - 93.45 (°C)
pH of solution	5
Deposition time	1 (hour)
Activation temperature	55 (°C)
Bath Volume	250 (cm^3)

2.3. Electrochemical test

The corrosion behavior of the coated samples was examined by potentiodynamic polarization tests using potentiostat apparatus (Origalys) and 3.5 wt.% NaCl solution. The corrosive medium was used to simulate the seawater environment. With the help of potentiodynamic polarization measurements, the kinetics of cathodic and anodic reaction can be determined. A standard saturated calomel electrode (SCE) was used as a reference and a graphite rod was used as an auxiliary electrode. The open surface area of the electrolyte was 1 cm^2 for each substrate, and the tests were carried out at ambient temperature. The potential was scanned from −1.2 V to +0.4 V with a scanning rate of 1 mV/s. The polarization test was carried out after 2 hr of OCP (Open circuit potential) for each sample. Corrosion potential (E_{corr}) and exchange current density (I_{corr}) values were further obtained by the Tafel extrapolation method. The Tafel slope tells about the nature of the mechanism of the electrode reactions [25-27]. The polarization tests were carefully carried out to avoid any scratch in the coatings. The polarization parameters such as Corrosion Potential (E_{corr}), Corrosion Current Density (I_{corr}), cathodic Tafel slope (β_c) and anodic Tafel slope (β_a) of the optimized Ni-Co-P coatings were observed.

2.4. Characterization procedure of the as-deposited coating

In order to perform Optical Microscopy, the microscope that is used for the specimen illustration or obtaining the microstructure of the given samples is a Metallurgical microscope. A metallurgical microscope refers to a high power microscope used for the purposes of viewing opaque objects. The metallurgical microscope differs from the other microscopes in the method by which the specimen illustration is done. Frontal lighting is used in the metallurgical microscopes for illuminating the opaque metal surface. This is achieved by using a plain glass reflector that is installed inside the tube.

Scanning Electron Microscopy (SEM) is performed with the aid of the Scanning Electron Microscope which is a type of electron microscope that produces images of a sample by scanning the surface with a focused beam of electrons which scans the specimen surface in a vacuum, imaging one point at a time. The interaction of the electron beam with every point of the specimen surface is registered, forming the entire image. The signals used by a scanning electron microscope to produce an image result from interactions of the electron beam with atoms at various depths within the sample. Since the wavelength of the electron beam is much lower than the wavelength of the visible light, the magnification of SEM is much higher, nearly a thousand times more than that of the optical microscopes. The resolution of SEM is about 1nm to 30nm. The SEM analysis was performed on the SOF software, employing aJEOL-Jsm 7610F machine.

X-ray crystallography is a technique used for determining the atomic and molecular structure of a crystal, in which the crystalline atoms cause a beam of incident X-rays to diffract into many specific directions. By measuring the angles and intensities of these diffracted beams, a crystallographer can produce a three-dimensional picture of the density of electrons within the crystal. The basic law involved in the diffraction method of structural analysis is Bragg's law ($2d\ sin\theta = n\lambda$). Here d is the spacing between diffracting planes, θ is the incident angle, n is an integer, and λ is the wavelength of

the beam. These specific directions appear as spots on the diffraction pattern called reflections. Thus, X-ray diffraction results from an electromagnetic wave (the X-rays) impinging on a regular array of scatterers. The X-ray Diffraction (XRD) analysis was performed in RigakuUltima-III X-ray diffractometer using Cu Kα radiation with 2θ lying in the range 20-80^o along with a scan speed of 2^o min^{-1}.

2.5. Response Surface Methodology

Response Surface Methodology (RSM) is a collection of statistical and mathematical methods that are useful for modeling and analyzing engineering problems. In this technique, the main objective is to optimize a response surface that is influenced by various process parameters. RSM consists of a group of techniques used in designing an experimental study to establish the relationship between a response parameter and several input parameters. The main advantage of using RSM is to understand and evaluate the effect of multiple parameters and their interactions with each other in bringing out the response(s). Hence, it is considered as an appropriate approach to optimize a process with the multi-parameter system such as electroless coating deposition where the concentration of cobalt sulfate, the concentration of sodium hypophosphite and bath temperature were considered as input parameters and corrosion rate as the response parameter. CCD is an extensively used statistical method based on the multi-variant nonlinear model for the optimization of process variables. It is also used to measure the reversion of model equations and operating parameters from the appropriate experiments. CCD is a mathematical operation in which the response parameter (corrosion rate) and the individual levels of each input parameter are fed to the Design Expert Software. This gives a regression equation, showing the dependencies of the corrosion rate on the input parameters.

3. RESULTS AND DISCUSSION

3.1. Optimization of the process parameter using Central Composite Design (CCD)

Three important process parameters viz. cobalt sulfate ($CoSO_4.7H_2O$), sodium hypophosphite ($NaH_2PO_2.H_2O$) and bath temperature were considered for optimization. The amount of cobalt deposited is determined by the concentration of cobalt sulfate. The amount of cobalt deposited is one of the important parameters which controls the corrosion resistance offered by the coating. In the same way, phosphorus deposits are controlled by sodium hypophosphite. The temperature of the electroless bath controls the rate of reaction and deposition of the elements. Hence these parameters are important and varied for the design. The relation between the response and the process parameters equation formed is called the regression equation. Six central points were considered for the formation of a full factorial regression equation. The coded values of process parameters are given in Table 2.

Table 2: Coded values of process parameters

Actual Values			Coded Values		
Cobalt Sulfate(g/L)	**Sodium Hypophosphite(g/L)**	**Bath Temperature(ºC)**			
X1	**X2**	**X3**	**Z1**	**Z2**	**Z3**
6.56	16.44	76.55	$-\alpha$	$-\alpha$	$-\alpha$
10	19.86	80	-1	-1	-1
15	25	85	0	0	0
20	29.91	90	1	1	1
23.44	33.33	93.45	$+\alpha$	$+\alpha$	$+\alpha$

RSM (Response Surface Methodology) was chosen to investigate the problem both statistically and mathematically. Using a rotatable central composite design (CCD) of the experiment, the response surfaces were developed. The CCD encloses 8 factorial points, 6 central points, and 6 axial points. Corrosion testing was done for all such points. The observed data followed by CCD is given in Table 3.

Table 3: 20 Set of experimental variables of the central composite design (CCD)

Set of Experiments	Cobalt Sulfate (g/L)	Sodium Hypophosphite (g/L)	Bath temperature (°C)	Corrosion Rate (µm/Y)
1	20.00	20.00	90.00	0.6088
2	20.00	30.00	90.00	0.5690
3	15.00	25.00	85.00	0.9642
4	15.00	25.00	85.00	0.9382
5	15.00	25.00	85.00	0.9342
6	10.00	20.00	80.00	0.6236
7	10.00	30.00	90.00	0.3143
8	15.00	25.00	76.60	0.7121
9	15.00	25.00	85.00	0.9543
10	15.00	25.00	93.41	0.7121
11	15.00	25.00	85.00	0.9712
12	20.00	20.00	80.00	0.5643
13	15.00	25.00	85.00	0.9790
14	10.00	20.00	90.00	0.5254
15	23.40	25.00	85.00	0.4980
16	15.00	33.41	85.00	0.4340
17	15.00	16.60	85.00	0.9277
18	6.60	25.00	85.00	0.4243
19	10.00	30.00	80.00	0.3976
20	20.00	30.00	80.00	0.4101

The experimental results of the corrosion test of different sets of experiments as a coded form are given in Table 4.
The corrosion rate of the substrate was experimentally found to be 2.12 µm/Y.

Table 4: 20 Set of experimental variables of the coded value of central composite design (CCD)

Set of Experiments	Cobalt Sulfate	Sodium Hypophosphite	Bath temperature	Corrosion Rate (µm/Y)
1	+1	-1	+1	0.6088
2	+1	+1	+1	0.5690
3	0	0	0	0.9642
4	0	0	0	0.9382
5	0	0	0	0.9342
6	-1	-1	-1	0.6236
7	-1	+1	+1	0.3143
8	0	0	-α	0.7121
9	0	0	0	0.9543
10	0	0	+α	0.7121
11	0	0	0	0.9712
12	+1	-1	-1	0.5643
13	0	0	0	0.9790
14	-1	-1	+1	0.5254
15	+α	0	0	0.4980
16	0	+α	0	0.4340
17	0	-α	0	0.9277
18	-α	0	0	0.4243
19	-1	+1	-1	0.3976
20	+1	+1	-1	0.4101

The final central composite design (CCD) obtained for corrosion rate with significant terms was quadratic as suggested by the software analysis in the actual and coded equation, and is given as:

Final Equation in Terms of Coded Factors:

$$Corrosion\ Rate = 9.60 + 0.3 \times A - 1.07 \times B + 0.016 \times C + 0.3 \times A \times B + 0.48 \times A \times C + 0.16 \times B \times C - 1.95 \times A^2 - 1.18 \times B^2 - 1.07 \times C^2 \quad (1)$$

Final Equation in Terms of Actual Factors:

$$\text{Corrosion rate} = -298.97501 + 0.46689 \times \text{Cobalt Sulfate (CoSO4)} + 1.41025 \times \text{Sodium Hypophosphite (NaH2PO2)} + 6.81241 \times \text{Bath temperature} + 0.012155 \times \text{Cobalt Sulfate (CoSO4)} \times \text{Sodium Hypophosphite (NaH2PO2)} + 0.019245 \times \text{Cobalt Sulfate (CoSO4)} \times \text{Bath temperature} + 6.46500E-003 \times \text{Sodium Hypophosphite (NaH2PO2)} \times \text{Bath temperature} - 0.078193 \times \text{Cobalt Sulfate (CoSO4)}^2 - 0.047122 \times \text{Sodium Hypophosphite (NaH2PO2)}^2 - 0.042703 \times \text{Bath temperature}^2 \quad (2)$$

3.2. Corrosion Study

The potentiodynamic polarization test was carried out and the data achieved from this test are plotted as shown in Figure 1 (called the polarization curve). This Figure shows that the anodic current slope value will be much higher compared to the cathodic current slope. The Tafel slope tells about the nature of the mechanism of the electrode reactions. Figure 1 shows that anodic reactions are the main reason for the corrosion of the coatings. The polarization parameters, Corrosion Potential (E_{corr}), Corrosion Current Density (I_{corr}), cathodic Tafel slope (β_c) and anodic Tafel slope (β_a) of the optimized Ni-Co-P coatings are shown in Table 5. Aal *et al* [26] obtained similar a polarization curve and electrochemical data for the electroless Ni-Co-P deposits over Al alloy tested in a 3.5% NaCl solution.

Table 5: Polarization parameters of the optimized Ni-Co-P coating.

Polarization Parameters	Experimental Value
Corrosion Potential (E_{corr})	-414.95 mV
Corrosion Current Density (I_{corr})	22.32 µA
Cathodic Tafel slope (β_c)	74.4 mV
Anodic Tafel slope (β_a)	200.2 mV

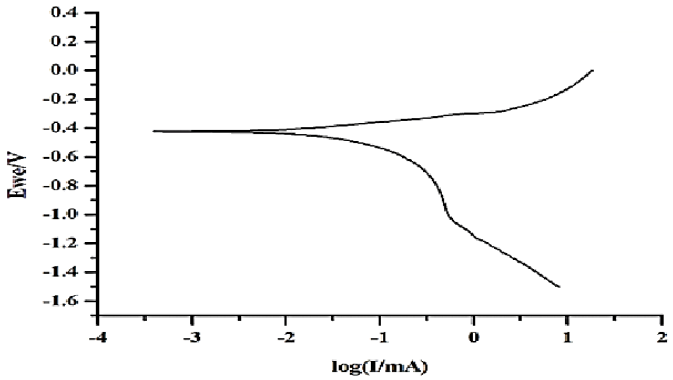

Figure 1: Potentiodynamic polarization curve for Ni-Co-P coating

The I_{corr} of the Copper Substrate was found to be 202.8 µA. Hence the efficiency of the coating will be given by $\eta = \frac{I_{corr}^{substrate} - I_{corr}^{coating}}{I_{corr}^{substrate}}$. So the efficiency of the coating is 89%.

The Electrochemical Impedance Spectroscopy (EIS) of the optimized sample was done. The Nyquist Impedance plot of the optimized sample that was obtained through EIS is shown in Figure 2.

The Nyquist plot was made to fit in the Randle's Circuit. Randle's circuit represents the whole corroding medium and the coating. Rs is the solution resistance formed in the electrolytic NaCl solution.

Rct is the total resistance of the system (coating + solution). The resistance of the coating is given their difference. Rct is formed due to oppositely charged ions transferring from the coating and electrolytic medium sides. The Randle's circuit contains Rs in series with Rct and CPE (Constant Phase Element) in parallel. The Nyquist plot in Figure 2 has one capacitive loop. So the electrochemical process is controlled by charge transfer. The use of a CPE comes into play because of the double layer formed at the solution/coating interface. This double layer is formed due to the non-homogeneity of the deposits or irregularities on the surface. Due to CPE, Capacitance is formed as double-layer capacitance when one liquid medium is in contact with the solid medium and oppositely charged ions are flowing from different sides and a voltage is applied across it, which makes it behave as a capacitor The Randle's Circuit is shown in Figure 3.

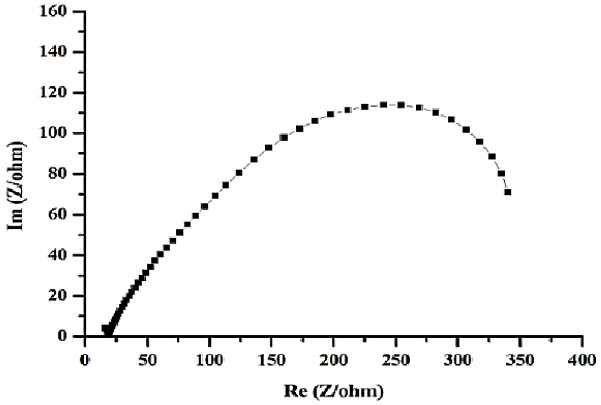

Figure 2: Nyquist Impedance plot of the Ni-Co-P optimized coating in 3.5 % NaCl solution

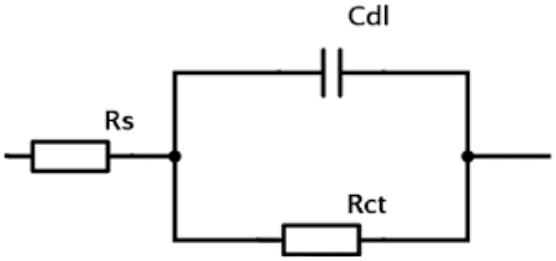

Figure 2: Randles Circuit

3.3. Analysis of Variance (ANOVA)

The corrosion rate is obtained from testing the polarization test of potentiodynamic and the rate of corrosion rate is determined by the surface response method (RSM) with central composition design (CCD). Considering the values of all the parameters of ANOVA statistical result of the model was found to be significant in this work. The model designed on all the experiments is carried out by using the design expert 9 software and it followed a second-order quadratic equation to calculate the optimum corrosion rate.

The maximum corrosion rate was found in Experiment 13 which is a combination of a cobalt sulfate ($CoSO_4$) concentration of 15 g/L, a sodium hypophosphite (NaH_2PO_2) concentration of 25 g/L and a bath temperature of 85 °C. Meanwhile, the minimum corrosion rate is obtained in Experiment 7 which is a combination of cobalt sulfate ($CoSO_4$) concentration of 10g/L, sodium hypophosphite (NaH_2PO_2) concentration of 30g/L and a bath temperature of 90°C, which is given in Table 3. In order to find out the right combination of these process parameters for obtaining the lowest corrosion rate, the optimization analysis is evaluated with the aid of RSM (in this current study CCD is employed).

ANOVA is a powerful mathematical tool used to determine the significant parameters in a process taking place. It uses the concept of p-value and F-value to find significant factors. The p-value is a parameter by which we can choose to reject the null hypothesis. If the p-value is less than 0.05 then we can reject the null hypothesis (we can say that the parameter is significant). The F-value is the ratio of the summation of the square of the factors to the variance of the errors. Hence a higher value of F

will suggest a relatively better factor with respect to others. The CCD analysis result is given in Table 6 and Table 7.

Table 6: ANOVA for Response Surface Quadratic Model

Sum of Source	Sum of Squares	df	Mean Square	F-Value	p-value	Prob> F
Model	97.9	9	10.88	22.57	< 0.0001	significant
A-Cobalt Sulfate ($CoSO_4$)	1.26	1	1.26	2.62	0.1366	
B-Sodium Hypophosphite (NaH_2PO_2)	15.64	1	15.64	32.45	0.0002	
C-Bath temperature	3.51E-03	1	3.51E-03	7.29E-03	0.9337	
AB	0.74	1	0.74	1.53	0.2439	
AC	1.85	1	1.85	3.84	0.0784	
BC	0.21	1	0.21	0.43	0.5251	
A^2	55.07	1	55.07	114.28	< 0.0001	
B^2	20	1	20	41.51	< 0.0001	
C^2	16.42	1	16.42	34.08	0.0002	
Residual	4.82	10	0.48			
Lack of Fit	4.66	5	0.93	28.78	0.0011	significant
Pure Error	0.16	5	0.032			
Cor Total	102.72	19				

The Model F-value of 22.57 implies the model is significant. There is only a 0.01% chance that a "Model F-value" this large could occur due to noise. Values of "Prob > F" less than 0.0500 indicate model terms are significant. In this case, A^2, B^2, C^2 are significant model terms. The "Lack of Fit F-value" of 28.78 implies the Lack of Fit is significant. There is only a 0.11% chance that a "Lack of Fit F-value" this large could occur due to noise.

Table 7: ANOVA result of CCD design

Result of CCD design	Value
Std. Dev.	0.69
Mean	6.73
C.V. %	10.31
PRESS	35.66
R-Squared	0.9531
Adj R-Squared	0.9109
Pred R-Squared	0.6528
Adeq Precision	12.594

As per the table value, R^2 of 0.9531 is in reasonable agreement with the Adj R^2 of 0.9109 that is the difference is less than 0.2. Adeq precision measures the signal to noise ratio which should ideally be greater than 4. The coefficient of variance (CV) for the corrosion rate is calculated to be 10.31 %. Considering the values of all the parameters of the ANOVA statistical result shows the model is significant.

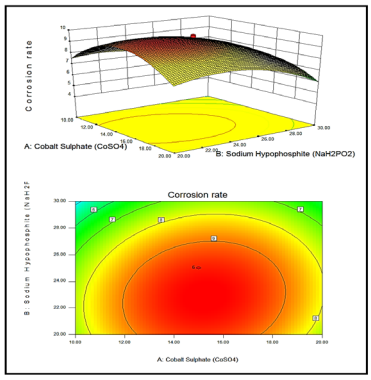

Figure 3: 2D-Contour plots and 3D-Response surface plots showing the effect of cobalt sulfate and sodium hypophosphite

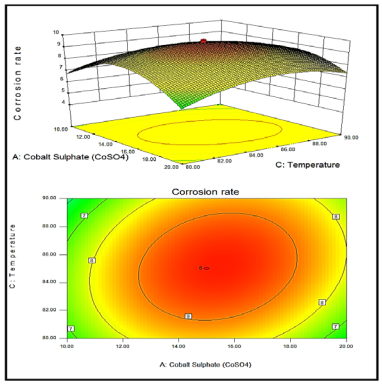

Figure 4:2D-Contour plots and 3D-Response surface plots showing the effect of cobalt sulfate and bath temperature

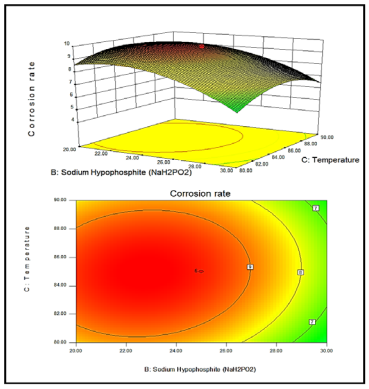

Figure 5:2D-Contour plots and 3D-Response surface plots showing the effect of sodium hypophosphite and bath temperatures

From Figure 4 it was observed through the 3D plot that with the increase of sodium hypophosphite and cobalt sulfate the corrosion rate increases up to a certain level then further it reduced, though the rate of reduction is very less. The contour plot represents two-dimension input and one dimension output.
After examination of Figure 5, it was observed that with the increase in cobalt substrate and bath temperature the corrosion rate decreases at a very high rate. This interaction between the X1 and X3 helps to reduce the corrosion rate to a desired value.

From Figure 6, we understood that with the increase in sodium hypophosphite and bath temperature the result is not desirable. The corrosion rate does not reduce as compared to other interactions.

From the equation and Figure 4, to Figure 6, it is apparent that the corrosion rate is highly affected by the interaction between the cobalt sulfate and bath temperature. However, the Sodium Hypophosphite is kept constant at 24.88 gm/l. At this relation the corrosion rate is minimum. Hence, the regression model (Equation 1) proposed in this work is acceptable.

Corrosion rate depends on the combination of the concentration of Cobalt Sulfate ($CoSO_4$), Sodium Hypophosphite (NaH_2PO_2) and bath temperature. From the analysis of the model, the intended corrosion rate is optimized based on the desirability function approach and desirability functions as a result of a combination of process variables.

The optimal condition was obtained at Cobalt Sulfate of 14.02 g/L, Sodium Hypophosphite of 29.57 g/L and a bath temperature of 80.38°C. Under the mentioned conditions, maximum incorporation i.e. corrosion rate was estimated to be 0.53501 µm/Y. Gao *et al*. [18] with a slightly different set of parameters achieved similar corrosion rates for Ni-Co-P alloy coatings. The decrease in the corrosion rate is from 2.12 to 0.53501 µm/Y.

Ashassi-Sorkhabi and Rafizadeh [27] studied the effect of coating time on the corrosion characteristics of Ni-P electroless deposits and the least corrosion rate achieved by them was 0.75µm/Y with 13.1 wt.% of Phosphorous. Zhao and Liu [28] compared the corrosion rates of Ni-P based coatings in HCl and NaCl solutions and from the graphs of corrosion rate versus the respective solution concentration, we can say that 0.8µm/Y was the least value of corrosion rate of Ni-P coating achieved by them. Thus the inclusion of Cobalt into the Ni-P matrix reduces the corrosion rate of the substrate by a significant amount.

3.4. Compare the experimental and model value analysis

According to the model, the 20 sets of experiments are conducted from which the experimental and model values are recorded on the basis of the extent of reduction which is given in Table 8. The deviation of the experimental results from values given by the model is found to be less than 1%.

Table 8: Compare the experimental and model value analysis

Set of Expt.	Expt. Values (µm/Y * 10)	Model Values (µm/Y * 10)	Error In Percentage
1	6.088	6.50959	-0.0042159
2	5.690	5.30059	0.0038941
3	9.642	9.43339	0.0020861
4	9.382	9.43339	-0.0005139
5	9.342	9.43339	-0.0009139
6	6.236	7.02169	-0.0078569
7	3.143	3.34369	-0.0020069
8	7.121	6.39338	0.0072761
9	9.543	9.43339	0.0010961
10	7.121	6.44000	0.0068100
11	9.712	9.43339	0.0027861
12	5.643	5.83859	-0.0019559
13	9.790	9.43339	0.0035661
14	5.254	5.76819	-0.0051419
15	4.980	4.18908	0.0079092
16	4.340	4.31086	0.0002914
17	9.277	7.90606	0.0137094
18	4.243	3.53909	0.0070391
19	3.976	3.95069	0.0002531
20	4.101	3.98309	0.0011791

Hence it can be concluded from the result that the experimental values properly match the model. Graphical analysis of experimental and model value with a set of reactions is given in Figure 7.

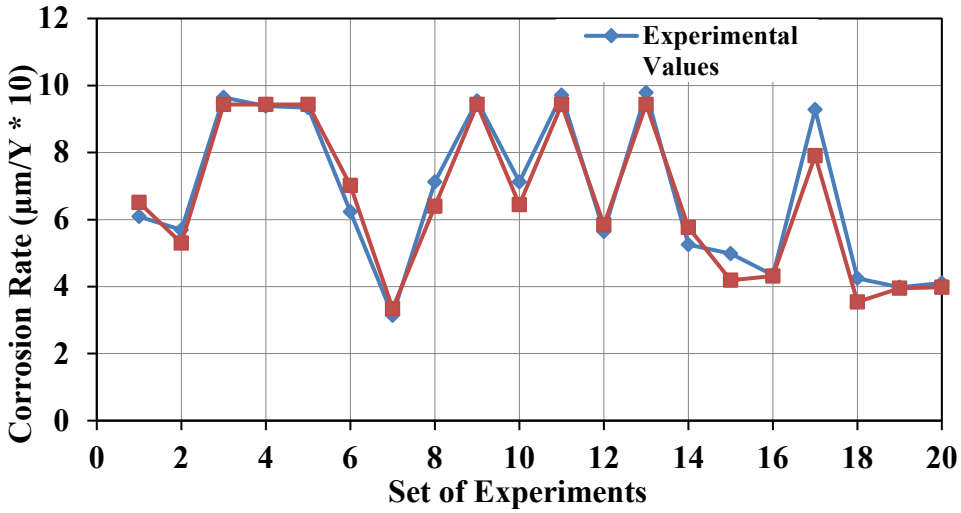

Figure 6: Graphical analysis of experimental and model value with a set of experiments

3.5. Characterization of experimental samples

The characterization of the experimental sample, before and after experimentation has been presented in the following sections.

3.5.1. The microstructure of the copper sample

Copper foils were taken for different experimentation. Under SEM, the grains in the samples are oriented longitudinally along the stretch forming direction most preferentially. The confirmation of the directionality has been substantiated (Figure 8).

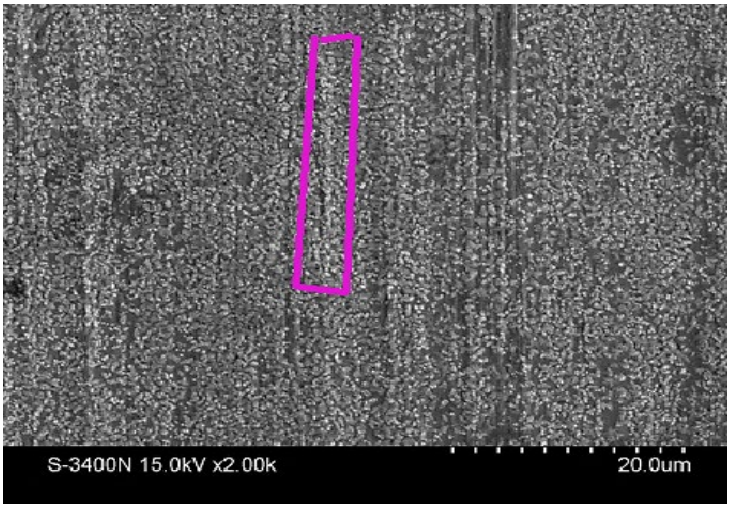

Figure 8. The directionality of deformed grains are visible in unetched SEM microstructure

3.5.2. Microstructures of as-deposited Optimize Coated Sample

Round particles in a continuous manner were observed under an optical microscope (Figure 9) in the case of the microstructures of optimized as-deposited coated samples. Some of the particles were of larger size though particle clustering was observed in some places.

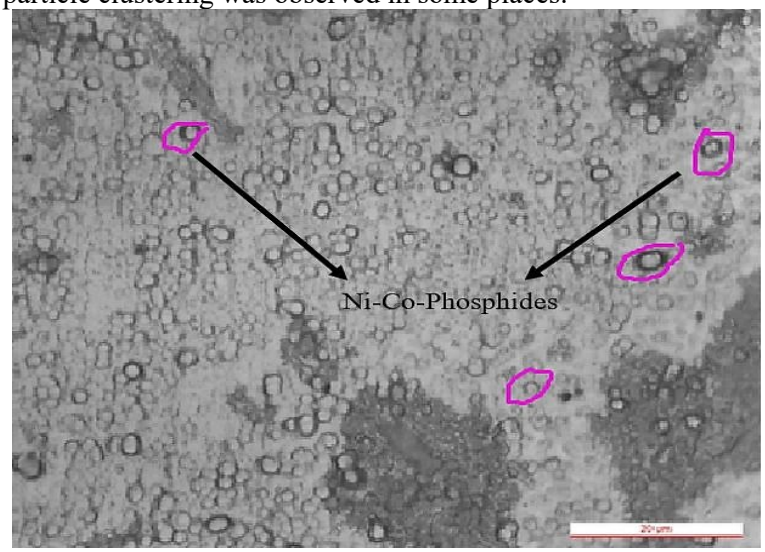

Figure 9: Optical Microstructure of electroless deposit on copper foil (Etchant $FeCl_3$ in dilute HCl)

Droplets of disc plate of Ni-Co-Phosphide's are observed on the surface (shown by pink).

Under SEM the characteristics of the electroless deposit have been further revealed (Figure 10). Close deposition of round particles is exposed distinctly though size variations from 2– 4 µm are common. Figure 10 shows no presence of cracks and holes on the surface of the coatings which suggests a highly compact coating with minimum defects was formed.

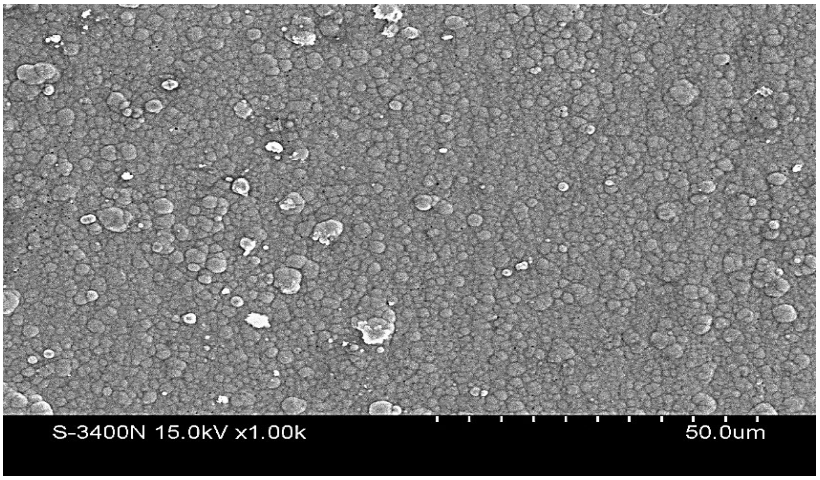

Figure 10: Scanning Electron Microscopy micrograph of the optimized as-deposited coated sample

The disintegration of the ovality of the electroless deposit can be visible in Figure 11. After corrosion, under SEM, the electroless deposits exhibit deterioration in the oval shape of the particles for the deposit. Sometimes those disintegrate randomly, though decomposition could not be established clearly. The presence of the intermetallic Ni_3P phase (as seen from XRD) in the matrix of the coating increases the hardness of the coating. This decreases the porosity of the coating [29] and doesn't allow the corroding medium to seep through the coating and reach the surface of the substrate. It can be clearly seen that the coating hasn't undergone much corrosion as no forms of disintegrations can be seen on the surface of the coating in Figure 11.

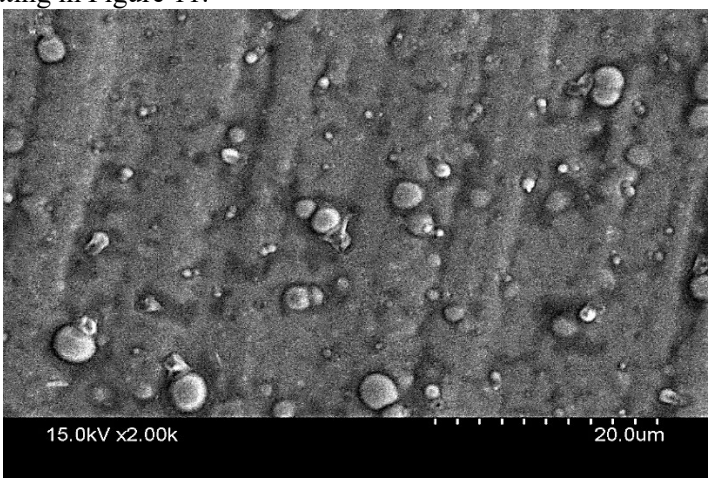

Figure 11: Scanning Electron micrograph of the optimized coating after corrosion testing. Under SEM, after the Corrosion experiment, the disintegration of oval shape for the electroless deposit can be visible.

The sectional microstructure of coated samples provided a rough estimate of the electroless Ni-Co-P coatings as shown in Figure 12. The measured thickness on an average appears to be 2 μm. The thickness is in accordance with the existing literature [30]. Figure 12 also reveals no presence of blowholes in the cross-section of the coating. This suggests that the coating deposition is very uniform and at the same time will have a higher resistance to corrosion since the corroding medium will be unable to reach the surface of the substrate through the coating.

Hou H *et al*. and Hu R *et al*. showed the presence of similar nodular deposition with no cracks and cervices [30,31]. The deposits in the optimized sample show no presence of cracks as well and covering the whole surface. The nodular structured deposits do not allow the corroding medium to seep into the substrate which increases the resistance offered by the coating, thereby decreasing its corrosion rate.

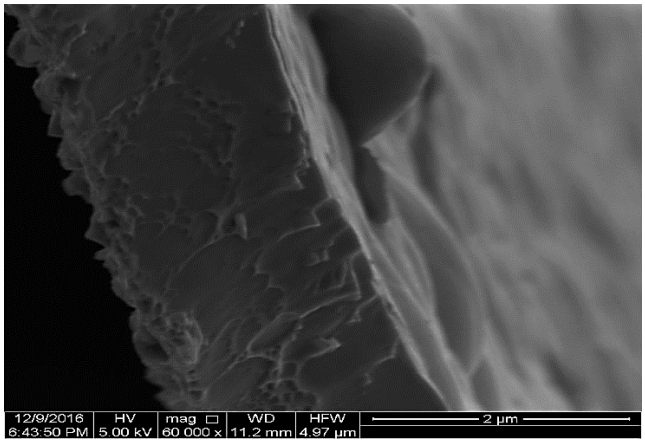

Figure 12: Cross-sectional view of as-deposited electroless Ni-Co-P coating by FESEM (Field Electron Scanning Electron Microscopy)

From EDX analysis as shown in Figure 13, the content of the coated deposit is Co -14.88 wt%, Ni-73.30 wt%, and P -14.88 wt%. This content of Cobalt is in association with previous pieces of literature having multiplied micro-hardness in comparison to the copper substrate.

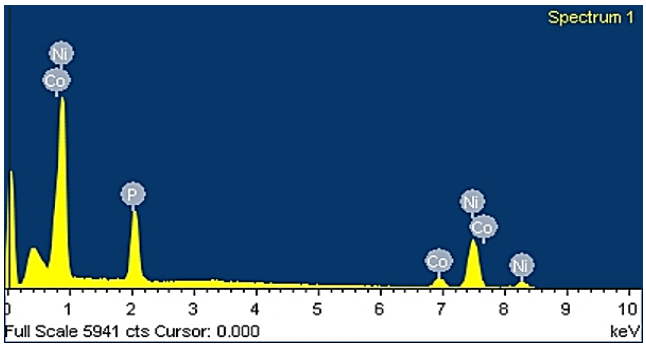

Figure 13: EDX optimized as-deposited Ni-Co-P coating

3.5.3. XRD of Copper substrate and deposit of Optimized Coated Sample

XRD analysis of the base coating material (Copper) is demonstrated in Figure 14. From the Figure, it can be concluded that the phase is FCC copper since it blatantly depicts only copper phase.

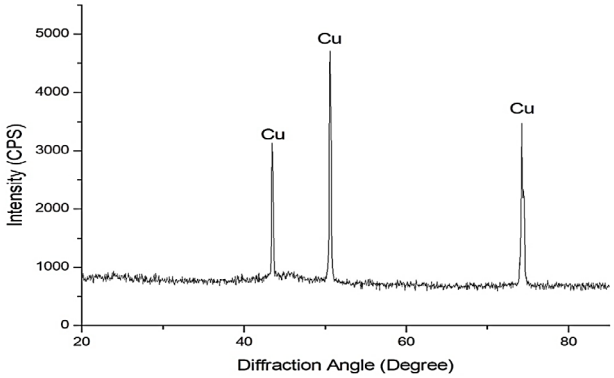

Figure 14: X-ray diffraction pattern of the copper substrate

XRD analysis of the optimized coated sample presented in Figure 15 it can be concluded that the major peaks of Ni_3P and a minor peak of Co_2P feature in the coating structure. The formation of the two phases (Ni_3P and Co_2P) fully depends on the concentration of cobalt sulfate ($CoSO_4$), the concentration of sodium hypophosphite (NaH_2PO_2) and the bath temperature. The presence of Ni_3P peaks in the coating

can be attributed to the reduction in the corrosion rate. In addition, a unique peak of Co_2P (previously obtained by Bi *et al.* in a similar electroless XRD spectra [32]) is observed in the coating could bring favorable properties to reduce the corrosion rate because from the literature, it is quite evident that the decrease in corrosion rate with the aid of Co_2P and Ni_3P phases is larger as compared to the decrease in corrosion rate only by the Ni_3P phase. The amount of phosphorus present in the coatings obtained from the EDX test reveals that it is a high phosphorus coating [3]. In case of high phosphorus coatings, Hadipour *et al*. showed the presence of various phases of Ni_xP_y at the diffraction angles similar to this study [33].

The reason for the improved properties can be drawn from the theory that the size of the phosphorus atoms is smaller in comparison to the cobalt and nickel atoms. The phosphorus atoms in the matrix acquire places of higher compressive stresses. The introduction of a new atom in the matrix introduces tensile stress. This neutralizes the internal compressive stresses and improving its mechanical properties.

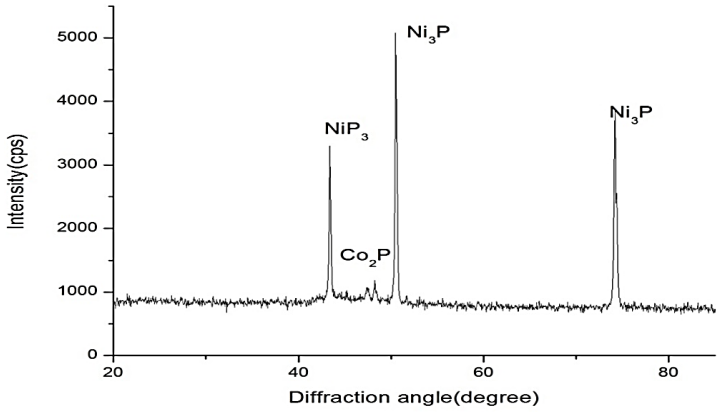

Figure 15: XRD pattern of as-deposited optimized Ni-Co-P alloy coating

4. CONCLUSION

The Response Surface Methodology (RSM) based on Central Composite Design (CCD) was used to evaluate and to optimize the effect of the process parameters cobalt sulfate($CoSO_4$. $7H_2O$)concentration, sodium hypophosphite ($NaH_2PO_2.H_2O$) concentration and bath temperature. From Equation 1 and Figure 2 to Figure 4, it is apparent that the corrosion rate is highly affected by the interaction between cobalt sulfate and the bath temperature. The optimal condition which led to the best incorporation of X1, X2, and X3 in the electroless bath, was obtained at 15 g/L of Cobalt Sulfate, 30 g/L of Sodium Hypophosphite, and 80°C of bath temperature. Under the mentioned conditions, the minimum corrosion rate of the as-deposited optimized coated sample was estimated to be 0.535 µm/Y. While the corrosion rate of the copper substrate was originally 2.12 µm/Y. Therefore, the rate of decrease in the corrosion rate due to the electroless deposit over the substrate was considered to be 74.76%. Close deposition of circular granular structures was revealed through SEM, the elemental compositions were revealed through EDX analysis and XRD analysis depicted the presence of three phases (Ni_3P, Co_2P and NiP_3). Results were in good agreement with the experimental and model values. Hence, this model can be a good cost-effective method for predicting the corrosion rates of electroless Ni-Co-P thereby saving time as well in industrial applications.

REFERENCES

[1] Shibli SMA, Chinchu KS. Development and electrochemical characterization of Ni-P coated tungsten incorporated electroless nickel coatings. Mater Chem Phys. 2016 Aug;178:21–30.
[2] Rezagholizadeh M, Ghaderi M, Heidary A, Vaghefi SMM. Electroless Ni-P/Ni-B-B4C duplex composite coatings for improving the corrosion and tribological behavior of Ck45 steel. Prot Met Phys Chem Surf. 2015 Mar;51(2):234–9.
[3] Biswas N, Baranwal RK, Majumdar G, Brabazon D. Review of duplex electroless coatings and their properties. Adv Mater Process Technol. 2018 Jul 3;4(3):448–65.

[4] Hryniewicz T, Rokosz K. Corrosion resistance of magnetoelectropolished AISI 316L SS biomaterial. Anti-Corros Methods Mater. 2014 Feb 25;61(2):57–64.
[5] Hassan N, Abdel Ghany NA. Corrosion of biomaterials: anodic treatment and evaluation of 316L stainless steel in simulated body fluid. Corros Eng Sci Technol. 2017 May 19;52(4):267–75.
[6] Elsener B, Alter M, Lombardo T, Ledergerber M, Wörle M, Cocco F, et al. A non-destructive in-situ approach to monitor corrosion inside historical brass wind instruments. Microchem J. 2016 Jan;124:757–64.
[7] Medgyes B, Tamasi P, Hajdu F, Muranyi R, Lakatos-Varsanyi M, Gal L, et al. Corrosion investigations on lead-free micro-alloyed solder alloys used in electronics. In: 2015 38th International Spring Seminar on Electronics Technology (ISSE) [Internet]. Eger, Hungary: IEEE; 2015 [cited 2019 Dec 20]. p. 296–9. Available from: http://ieeexplore.ieee.org/document/7248009/
[8] Huang T-H, Yang P-K, Lien D-H, Kang C-F, Tsai M-L, Chueh Y-L, et al. Resistive Memory for Harsh Electronics: Immunity to Surface Effect and High Corrosion Resistance via Surface Modification. Sci Rep. 2015 May;4(1):4402.
[9] Simonović A, Petrović M, Radovanović M, Milić S, Antonijević M. Inhibition of copper corrosion in acidic sulphate media by eco-friendly amino acid compound. Chem Pap [Internet]. 2014 Jan 1 [cited 2019 Dec 20];68(3). Available from: http://www.degruyter.com/view/j/chempap.2014.68.issue-3/s11696-013-0458-x/s11696-013-0458-x.xml
[10] Björkbacka Å, Johnson CM, Leygraf C, Jonsson M. Radiation Induced Corrosion of Copper in Humid Air and Argon Atmospheres. J Electrochem Soc. 2017;164(4):C201–6.
[11] Hosseinpour S, Göthelid M, Leygraf C, Johnson CM. Self-Assembled Monolayers as Inhibitors for the Atmospheric Corrosion of Copper Induced by Formic Acid: A Comparison between Hexanethiol and Hexaneselenol. J Electrochem Soc. 2014;161(1):C50–6.
[12] Cui X, Lin X, Liu C, Yang R, Zheng X, Gong M. Fabrication and corrosion resistance of a hydrophobic micro-arc oxidation coating on AZ31 Mg alloy. Corros Sci. 2015 Jan;90:402–12.
[13] Zhuang JJ, Guo YQ, Xiang N, Xiong Y, Hu Q, Song RG. A study on microstructure and corrosion resistance of ZrO2-containing PEO coatings formed on AZ31 Mg alloy in phosphate-based electrolyte. Appl Surf Sci. 2015 Dec;357:1463–71.
[14] Zhou H, Liao Z, Fang C, Li H, Feng B, Xu S, et al. Pulse electroplating of Ni-W-P coating and its anti-corrosion performance. Trans Nonferrous Met Soc China. 2018 Jan;28(1):88–95.
[15] Zhou S, Yang J, Li W, Jiang Q, Luo Y, Zhang D, et al. Preparation and Photovoltaic Properties of Ternary $AgBiS_2$ Quantum Dots Sensitized TiO_2 Nanorods Photoanodes by Electrochemical Atomic Layer Deposition. J Electrochem Soc. 2016;163(3):D63–7.
[16] Sumrunronnasak S, Tantayanon S, Kiatgamolchai S. Influence of layer compositions and annealing conditions on complete formation of ternary PdAgCu alloys prepared by sequential electroless and electroplating methods. Mater Chem Phys. 2017 Jan;185:98–103.
[17] Rabizadeh T, Allahkaram SR, Zarebidaki A. An investigation on effects of heat treatment on corrosion properties of Ni–P electroless nano-coatings. Mater Des. 2010 Aug;31(7):3174–9.
[18] Gao Y, Huang L, Zheng ZJ, Li H, Zhu M. The influence of cobalt on the corrosion resistance and electromagnetic shielding of electroless Ni–Co–P deposits on Al substrate. Appl Surf Sci. 2007 Oct;253(24):9470–5.
[19] Luo H, Leitch M, Zeng H, Luo J-L. Characterization of microstructure and properties of electroless duplex Ni-W-P/Ni-P nano-ZrO2 composite coating. Mater Today Phys. 2018 Mar;4:36–42.
[20] Sankara Narayanan TSN, Selvakumar S, Stephen A. Electroless Ni–Co–P ternary alloy deposits: preparation and characteristics. Surf Coat Technol. 2003 Jul;172(2–3):298–307.
[21] Parente MMV, Mattos OR. Electrochemical characterization of Ni±P and Ni±Co±P amorphous alloy deposits obtained by electrodeposition. :7.
[22] Hong S, Wu Y, Wang B, Zheng Y, Gao W, Li G. High-velocity oxygen-fuel spray parameter optimization of nanostructured WC–10Co–4Cr coatings and sliding wear behavior of the optimized coating. Mater Des. 2014 Mar;55:286–91.

[23] Díaz B, Freire L, Mojío M, Nóvoa XR. Optimization of conversion coatings based on zinc phosphate on high strength steels, with enhanced barrier properties. J Electroanal Chem. 2015 Jan;737:174–83.
[24] Chen L, Xia C, Qian P-Y. Optimization of antifouling coatings incorporating butenolide, a potent antifouling agent via field and laboratory tests. Prog Org Coat. 2017 Aug;109:22–9.
[25] Sarkar S, Baranwal RK, Lamichaney S, Majumdar G. Optimization of electroless Ni-Co-P coating with hardness as response parameter: A computational approach. 2018;17.
[26] Aal AA, Shaaban A, Hamid ZA. Nanocrystalline soft ferromagnetic Ni–Co–P thin film on Al alloy by low temperature electroless deposition. Appl Surf Sci. 2008 Jan;254(7):1966–71.
[27] Ashassi-Sorkhabi H, Rafizadeh SH. Effect of coating time and heat treatment on structures and corrosion characteristics of electroless Ni–P alloy deposits. Surf Coat Technol. 2004 Jan;176(3):318–26.
[28] Zhao Q, Liu Y. Comparisons of corrosion rates of Ni–P based composite coatings in HCl and NaCl solutions. Corros Sci. 2005 Nov;47(11):2807–15.
[29] Huang ZH, Zhou YJ, Nguyen TT. Study of nickel matrix composite coatings deposited from electroless plating bath loaded with TiB2, ZrB2 and TiC particles for improved wear and corrosion resistance. Surf Coat Technol. 2019 Apr;364:323–9.
[30] Hu R, Su Y, Liu H. Deposition behaviour of nickel phosphorus coating on magnesium alloy in a weak corrosive electroless nickel plating bath. J Alloys Compd. 2016 Feb;658:555–60.
[31] Huo H, Li Y, Wang F. Corrosion of AZ91D magnesium alloy with a chemical conversion coating and electroless nickel layer. Corros Sci. 2004 Jun;46(6):1467–77.
[32] Bi S, Zhao H, Hou L, Lu Y. Comparative study of electroless Co-Ni-P plating on Tencel fabric by Co0-based and Ni0-based activation for electromagnetic interference shielding. Appl Surf Sci. 2017 Oct;419:465–75.
[33] Hadipour A, M. Monirvaghefi S, Bahrololoom ME. Electroless deposition of graded Ni–P coatings. Surf Eng. 2015 Jun;31(6):399–405.